COLD SPRING HARBOR
Molecular Case Studies

RESEARCH ARTICLE

Somatic overgrowth associated with homozygous mutations in both *MAN1B1* and *SEC23A*

Swati Gupta,[1] Somayyeh Fahiminiya,[1] Tracy Wang,[1] Laura Dempsey Nunez,[1] David S. Rosenblatt,[1,2] William T. Gibson,[3] Brian Gilfix,[4] John J. M. Bergeron,[4] and Loydie A. Jerome-Majewska[1,2,5]

[1]Department of Human Genetics, McGill University, Montreal, Quebec H3A 1B1, Canada; [2]Department of Pediatrics, McGill University, Montreal, Quebec H4A 3J1, Canada; [3]Department of Medical Genetics, Child and Family Research Institute, Vancouver, British Columbia V6H 3V4, Canada; [4]Department of Medicine, McGill University, Montreal, Quebec H4A 3J1, Canada; [5]Department of Anatomy and Cell Biology, McGill University, Montreal, Quebec H3A 0C7, Canada

Abstract Using whole-exome sequencing, we identified homozygous mutations in two unlinked genes, *SEC23A* c.1200G>C (p.M400I) and *MAN1B1* c.1000C>T (p.R334C), associated with congenital birth defects in two patients from a consanguineous family. Patients presented with carbohydrate-deficient transferrin, tall stature, obesity, macrocephaly, and malocclusion teeth. The parents were healthy heterozygous carriers for both mutations and an unaffected sibling with tall stature carried the heterozygous mutation in *SEC23A* only. Mutations in *SEC23A* are responsible for craniolenticosultura dysplasia (CLSD). CLSD patients are short, have late-closing fontanels, and have reduced procollagen (pro-COL1A1) secretion because of abnormal pro-COL1A1 retention in the endoplasmic reticulum (ER). The mutation we identified in *MAN1B1* was previously associated with reduced MAN1B1 protein and congenital disorders of glycosylation (CDG). CDG patients are also short, are obese, and have abnormal glycan remodeling. Molecular analysis of fibroblasts from the family revealed normal levels of SEC23A in all cells and reduced levels of MAN1B1 in cells with heterozygous or homozygous mutations in *SEC23A* and *MAN1B1*. Secretion of pro-COL1A1 was increased in fibroblasts from the siblings and patients, and pro-COL1A1 was retained in Golgi of heterozygous and homozygous mutant cells, although intracellular pro-COL1A1 was increased in patient fibroblasts only. We postulate that increased pro-COL1A1 secretion is responsible for tall stature in these patients and an unaffected sibling, and not previously discovered in patients with mutations in either *SEC23A* or *MAN1B1*. The patients in this study share biochemical and cellular characteristics consistent with mutations in *MAN1B1* and *SEC23A*, indicating a digenic disease.

[Supplemental material is available for this article.]

Corresponding author: loydie.majewska@mcgill.ca

Ontology terms: childhood-onset truncal obesity; downslanted palpebral fissures; hypertelorism; macrocephaly at birth; moderate global developmental delay; proportionate tall stature

Published by Cold Spring Harbor Laboratory Press

doi: 10.1101/mcs.a000737

INTRODUCTION

Missense mutations in Sec23 homolog A (*SEC23A;* OMIM #610511) are associated with craniolenticosultura dysplasia (CLSD) (OMIM #607812) (Boyadjiev et al. 2006, 2011). CLSD is an autosomal-recessive disease characterized by late-closing fontanels, sutural cataracts, facial dysmorphism, and skeletal defects (Boyadjiev et al. 2006, 2011). The gene encodes for SEC23A, a GTPase-activating protein (GAP) for SAR1 that regulates COPII coat protein

assembly and disassembly (Yoshihisa et al. 1993; Lord et al. 2011). *SEC23A* mutant fibroblasts exhibit significantly distended endoplasmic reticulum (ER) membranes and abnormal retention of procollagen1, the precursor of COL1A1, in the ER. COL1A1 is the major extracellular component of bone. COPII coat assembly is also perturbed in *SEC23A* mutant fibroblasts (Boyadjiev et al. 2006, 2011; Kim et al. 2012).

Mutations in mannosidase alpha class 1B member 1 or *MAN1B1* (ERMan1) (OMIM #604346) are associated with both nonsyndromic autosomal-recessive intellectual disability (NS-ARID, mental retardation, OMIM #614202) and congenital disorders of glycosylation (CDG) (Rafiq et al. 2011; Rymen et al. 2013). MAN1B1 localizes to the Golgi and is required for N-glycan trimming of terminal mannose from the middle branch of asparagine linked $Man_9GlcNAc_2$ (Man9) to $Man_8GlcNAc_2$ (Man8) (Pan et al. 2013; Smirle et al. 2013). MAN1B1 activity generates an ER-associated degradation (ERAD) signal in yeast and mammalian cells that is essential in glycoprotein quality control (Pan et al. 2011). Most missense mutations decrease levels of the protein and/or reduce enzymatic activity of MAN1B1 (Rafiq et al. 2011; Rymen et al. 2013). Reduced enzymatic activity leads to deficient processing of N-linked glycans and delayed processing of Man9 to Man8 (Rymen et al. 2013; Van Scherpenzeel et al. 2014). MAN1B1 is also required for retention, recycling, and ERAD of misfolded proteins in an enzyme-independent manner (Pan et al. 2013; Iannotti et al. 2014). MAN1B1 interacts with the terminally misfolded null Hong Kong (NHK) variant of α-trypsin, an ERAD substrate. NHK is abnormally secreted in cells with knockdown of *MAN1B1*, and expression of a truncated MAN1B1 protein that is missing the enzymatic domain restores ERAD of this abnormally folded protein. In addition, fibroblasts from patients with mutations in this gene have dilated and fragmented Golgi membranes (Rymen et al. 2013).

We identified a novel mutation in *SEC23A* and a previously reported mutation in *MAN1B1* in two patients from a consanguineous family of Lebanese origin. The patients presented with moderate global developmental delay, tall stature, obesity, macrocephaly, mild dysmorphic features, hypertelorism, malocclusion teeth, intellectual disability, and flat feet. The mutations identified did not affect levels of SEC23A protein. Although levels of SEC23A did not change, cells with heterozygous mutation in *SEC23A* or *SEC23A* and *MAN1B1* had dilated ER and reduced Golgi-associated vesicles. In addition to these abnormalities, cells with heterozygous mutations in *MAN1B1* and *SEC23A* had abnormal retention of pro-COL1A1 in the Golgi. The ER was dilated and Golgi-associated vesicles were reduced in patient fibroblasts, similar to cells from unaffected members of the family, but these fibroblasts also had increased intracellular levels of pro-COL1A1. In contrast, fibroblasts with heterozygous and homozygous mutations in both *SEC23A* and *MAN1B1* had a significant decrease in levels of MAN1B1. Nonetheless, only the patients had a type 2-transferrin pattern and a significant increase of trisialotransferrin. These latter findings are consistent with an intrinsic defect of N-glycan remodeling. We propose that the abnormalities uncovered here, a combination of abnormal N-glycan remodeling and procollagen transport, contribute to phenotypic findings in these patients.

RESULTS

Clinical Phenotype and Family History

The family under consideration consists of two unaffected consanguineous first cousin parents, an unaffected daughter, and two affected sons (Fig. 1P). Affected patients presented with a developmental phenotype that was characterized by moderate global developmental delay, tall stature, obesity, macrocephaly, mild dysmorphic features, hypertelorism, malocclusion teeth, intellectual disability, and flat feet (Table 1; Fig. 1A–O).

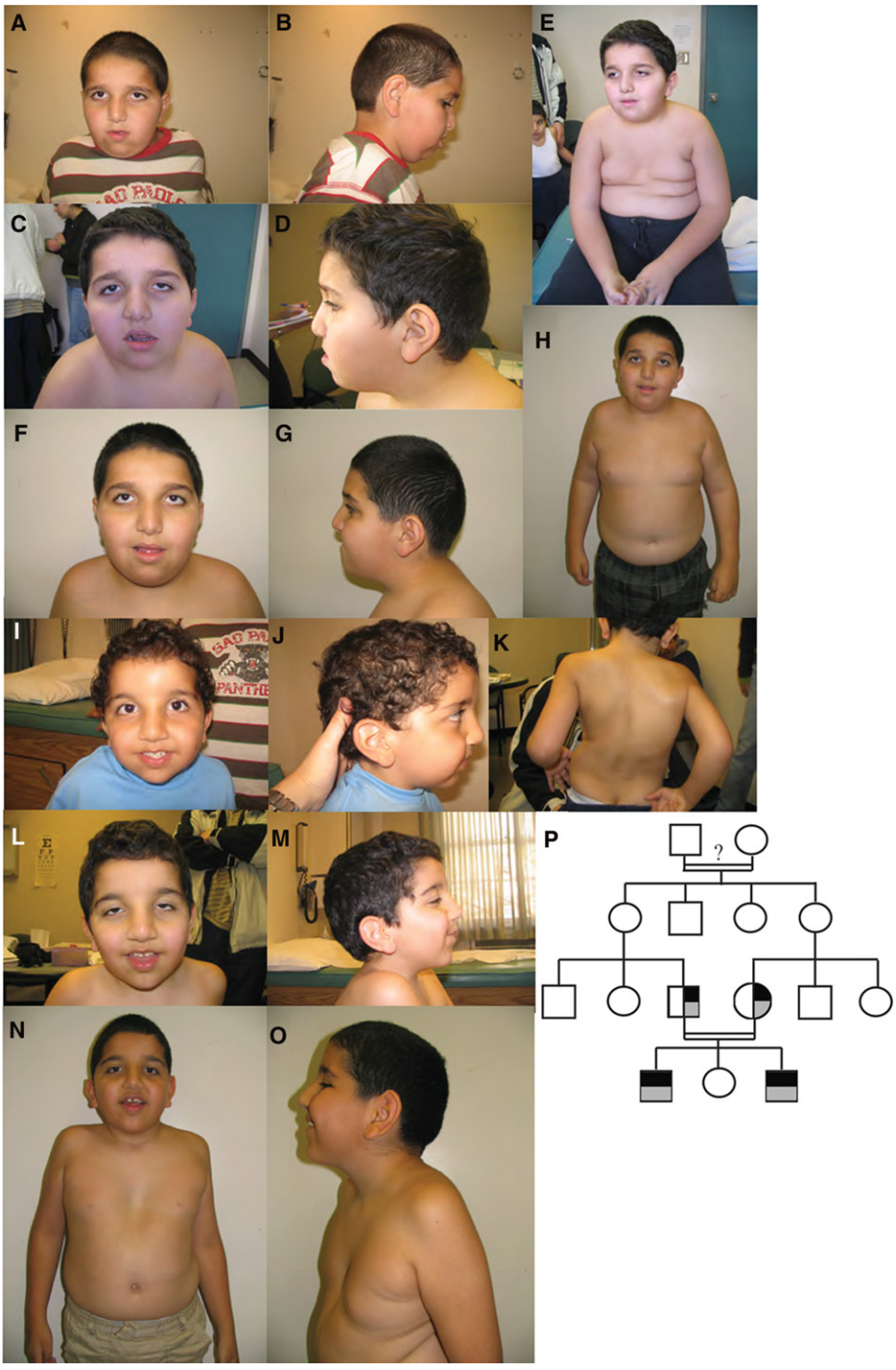

Figure 1. Photographs of Patient 1 at ages 7 yr (*A*,*B*), 8 yr + 7 mo (*C*–*E*), and 11 yr (*F*–*H*), and Patient 2 at ages 3 yr + 1 mo (I,J), 4 yr + 8 mo (*K*–*M*), and 7 yr + 2 mo (*N*, *O*). (*P*) Pedigree shows parents are first cousins, although more remote degrees of consanguinity between ancestral generations were thought to exist also. Black infill indicates carrier status for the familial *MAN1B1* mutation; gray infill indicates carrier status for the familial *SEC23A* mutation. Affected individuals have inherited two copies of both mutations. The clinically unaffected daughter is not homozygous for either mutation; because she has not yet reached the age of reproductive decision-making, her carrier status has not yet been disclosed to her parents.

Table 1. Clinical features of patients with *SEC23A*$^{M400I/M400I}$ *MAN1B1*$^{R334C/R334C}$ mutations and members of their family

Clinical features	P1	P2
Current age	14 yr, 1 mo	11 yr, 2 mo
Sex	M	M
Ancestry	Palestinian	Palestinian
Intellectual disability	Moderate	Moderate
Age of independent walking	18 mo	18 mo
Delayed speech development	+	+
Hypotonia	+	+
Birth weight (kilograms) and gestational age (weeks)	5.0 kg (41.5 wk)	3.6 (40 wk)
Macrocephaly[a,b]	+	+
Plagiocephaly	Mild (normal head CT)	Mild (head CT not done)
Tall stature[c]	+ (Height SDS 2.10, 172 cm, 86th percentile)	+ (Height SDS 1.00, 157 cm, 97th percentile)
Obesity[d]	+ (BMI SDS 4.20)	+ (BMI SDS 2.57)
Hypertelorism	+	+
Downslanting palpebral fissures	+	+
Long palpebral fissures	+	+
Ptosis	+	+
Large ears	+	+
Low-set ears	+	–
Hearing loss	Unilateral, mild	–
Nose shape	Prominent bridge and root ("tubular" shape)	Prominent bridge and root ("tubular" shape)
Hypoplastic nasolabial fold	+	+
Thin lateral upper lip	+	+
"Cupid's bow" mouth	+	+
Malocclusion	+	+
Palate	High arched	Normal
Prognathism	+	–
Vocal cord nodules	+	–
Hypernasal voice	+	–
Asymmetric nipples	+ (Not inverted)	–
Pectus excavatum	–	+
Scoliosis	–	+
Rib-bearing vertebrae	Normal	11 Pairs only
Joint hypermobility	–	+
Flat feet	+	+
Neonatal feeding difficulties	+	–
Reflux esophagitis	–	+
Inguinal hernia	–	+
Anal fissures/sinuses	+	–
Staring spells	+	+
EEG	Dysrhythmic background	Not done

Continued

Table 1. *Continued*

Clinical features	P1	P2
Myelination	Delayed	MRI not done
Bone age (age measured)	+1 SD (2.5 yr)	Not done

P1, Patient 1; P2, Patient 2; yr, years; mo, months; w, weeks; BMI, body mass index; CT, computed tomography; SD, standard deviation; SDS, standard deviation score (number of SD above the mean for age). "+" indicates presence and "−" indicates absence of phenotype.
[a]Macrocephaly was significant—Patient 1's head circumference was 55.0 cm at 3 yr, 8 mo, 57.7 cm at 7 yr, 58.6 cm at 8 yr, 7 mo, and 60.5 cm at 11 yr; Patient 2's head circumference was 55.5 cm at 3 yr, 1 mo, 56.5 cm at 4 yr, 8 mo, and 58.2 cm at 7 yr, 1 mo.
[b]The sister was clinically unaffected for all of the features outlined above except macrocephaly (head circumference 55.0 cm at age 9 yr, 2 mo, 97th percentile); she was 163 cm at age 13 yr, 2 mo (94th percentile) and has absence seizures, for which she takes valproic acid and ethosuximide.
[c]Parental head circumferences were at the 40th and 70th percentiles for the father and mother, respectively. Parental heights were at the 90th (182 cm) and 35th (162 cm) percentiles for the father and mother, respectively.
[d]Parental weights were within the normal, nonobese range.

Genomic Analyses

Based on the family history of consanguinity and the lack of other obvious etiological factors, we presumed an underlying genetic cause for the features found in affected patients. Thus, whole-exome sequencing (WES) was performed to interrogate their genomes for rare variants that might be responsible for their phenotype. Shared, homozygous nonsynonymous coding mutations were identified in five genes: *MUM1L1*$^{c.284G>A}$, *SASH3*$^{c.790A>G}$, *SEC23A*$^{c.1200G>C}$, *NUP214*$^{c.2701C>T}$, and *MAN1B1*$^{c.1000C>T}$ (dbSNP, rs387906886) (Table 2; Supplemental Table 1).

The mutation found in *MUM1L1* was previously reported and had a minor allele frequency of 0.003. However, mutations identified in *SASH3*, *SEC23A*, *NUP214*, and *MAN1B1* were rare and not previously seen in our exome database (>1400 exomes), in dbSNP (Database for Short Genetic Variations), in 1000 Genomes Project, nor in the NHLBI (National Heart, Lung, and Blood Institute) exome databases, with minor allele frequencies of 0 (Table 2). Three independent bioinformatics algorithms, SIFT, PolyPhen-2, and MutationTaster predicted both the 284G>A *MUM1L1* and the 2701C>T *NUP214* mutations as benign, suggesting that mutations in these genes are unlikely to be responsible for abnormalities found in our affected patients. The 790A>G *SASH3* mutation was predicted to be benign by SIFT, possibly damaging by PolyPhen-2 ($P = 0.463$), and damaging by MutationTaster ($P = 0.999$). *Sash3* is preferentially expressed in lymphoid tissues, and mutation of this gene in mouse indicates that it is required for generation of adaptive immune responses. Furthermore, although mice with mutation in *Sash3* have smaller lymphoid organs, reduced T-cell proliferation and cytokine production, and reduction of marginal zone B cells (Beer et al. 2005), they are

Table 2. List of genes with homozygous nonsynonymous coding mutations in both Patients 1 and 2 after whole-exome sequencing

Gene symbol	Gene name	Chr	Transcript	Nucleotide change	Protein change	Minor allele frequency
MUM1L1	melanoma associated antigen (mutated) 1-like 1	X	NM_001171020	c.284G>A	p.G95D	0.003
SASH3	SAM and SH3 domain containing 3	X	NM_018990	c.790A>G	p.I264V	0
SEC23A	Sec23 homolog A (*Saccharomyces cerevisiae*)	14	NM_006364	c.1200G>C	p.M400I	0
NUP214	nucleoporin 214 kDa	9	NM_005085	c.2701C>T	p.P901S	0
MAN1B1	mannosidase alpha, class 1B member 1	9	NM_016219	c.1000C>T	p.R334C	0

Table 3. Clinical features shared by patients in this study compared with previously reported features of patients with mutations in either *SEC23A* (Boyadjiev et al. 2006, 2011) or *MAN1B1* (Rafiq et al. 2011; Rymen et al. 2013)

Clinical features	*SEC23A;MAN1B1*	*SEC23A*	*MAN1B1*
Developmental delay	+	+	+
Hypotonia	+	–	+
Macrocephaly	+	–	+
Plagiocephaly	Mild (normal head CT)	NA	NA
Stature	**Tall**	**Short**	**Short**
Obesity	+	–	+
Hypertelorism	+	+	+
Downslanting palpebral fissures	+	+	+
Ptosis	+	NA	NA
Large ears	+	–	+
Nose shape	Prominent bridge and root ("tubular" shape)	Prominent bridge and slightly anteverted nares	Prominent
Hypoplastic nasolabial fold	+	NA	+
Thin upper lip	+	+	+
"Cupid's bow" mouth	+	NA	NA
Teeth	**Malocclusion**	**Delayed eruption and dental caries**	–
Flat feet	+	+	–
Staring spells	+	NA	NA

Features in bold are specific to patients in this study.
+, presence; –, absence; NA, clinical features not assessed; CT, computed tomography.

morphologically normal. Therefore, we assume that mutation in this gene cannot explain phenotypic abnormalities in the affected patients.

Both the 1200G>C mutation in *SEC23A* and the 1000C>T mutation in *MAN1B1* were within highly conserved residues and were predicted to be damaging by all three different bioinformatics algorithms ($P = 0.999$) (Supplemental Figs. S1and S2). In addition, Patients 1 and 2 shared a region of homozygosity of 7.5 Mb length on Chromosome 9 and 21 Mb on Chromosome 14, surrounding the identified mutations (Supplemental Fig. S3). Furthermore, because a subset of abnormalities found in our affected patients were previously reported in patients with mutations in either *SEC23A* or *MAN1B1* (Table 3; Boyadjiev et al. 2006, 2011; Rafiq et al. 2011; Rymen et al. 2013), we postulated that both *SEC23A* and *MAN1B1* mutations contribute to clinical findings in these patients.

Phenotypic Analyses

The 1000C>T mutation in *MAN1B1* is associated with N-glycan remodeling defect (Rymen et al. 2013); therefore, we performed capillary zone electrophoresis (Parente et al. 2010) on serum from an unaffected sibling heterozygous for the *SEC23A* mutant allele only, unaffected carriers heterozygous for mutations in both *SEC23A* and *MAN1B1*, and the affected patients. A normal transferrin pattern was found in all unaffected family members (Fig. 2A,B), whereas both patients had a type 2 transferrin pattern with significant increase in trisialotransferrin (incomplete biantennary forms, ranging from 44% to 48% of the transferrin forms)

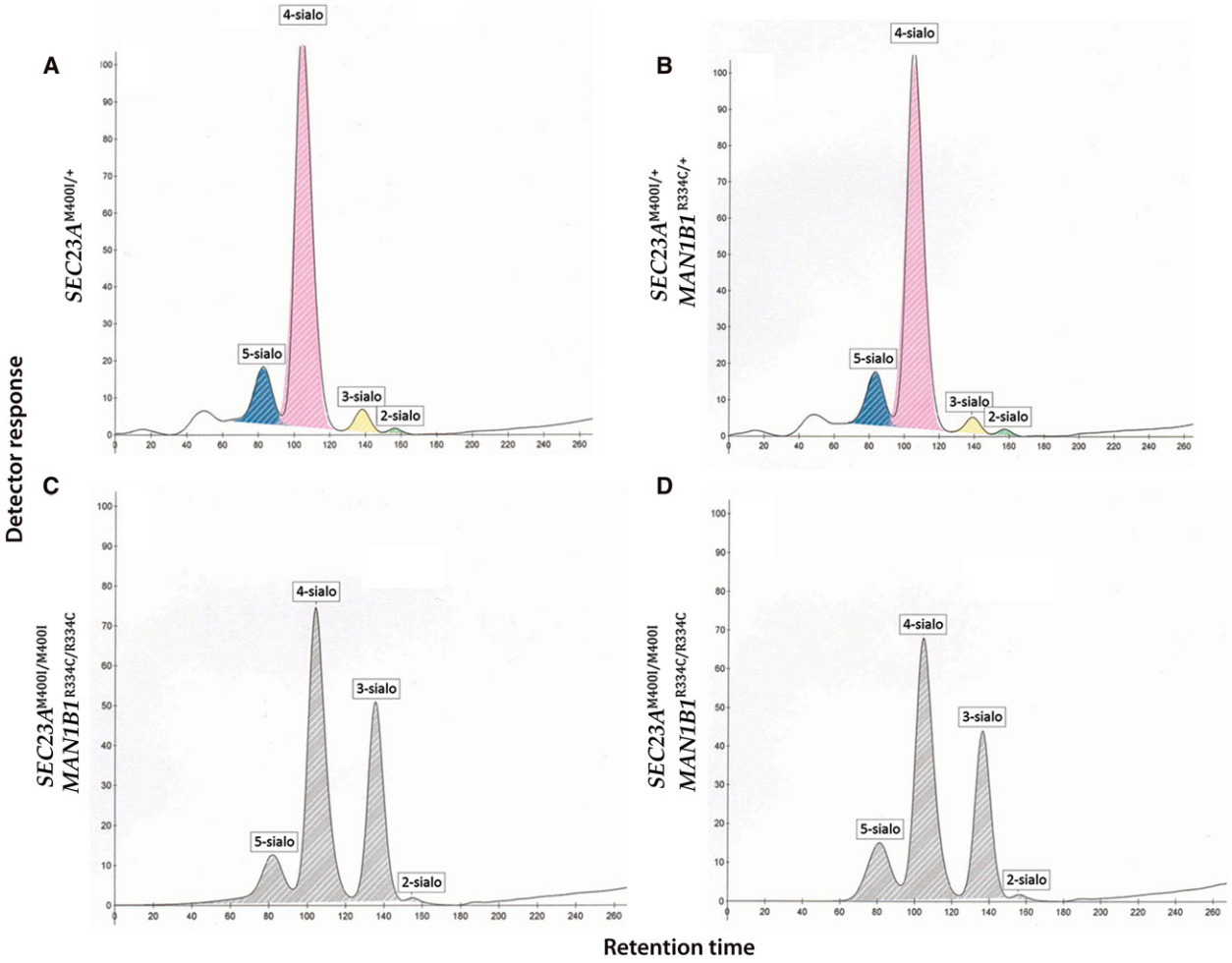

Figure 2. Trisialotransferrin, a type 2 transferrin pattern, was observed in patient serum. Capillary zone electrophoresis was used to obtain the chromatogram of transferrin isoforms in (*A*) *SEC23A* $^{M400I/+}$ heterozygous; (*B*) *SEC23A*$^{M400I/+}$ *MAN1B1*$^{R334C/+}$ double heterozygous; (*C*,*D*) *SEC23A*$^{M400I/M400I}$ *MAN1B1*$^{R334C/R334C}$ double homozygous mutant serum. The vertical scale is detector response in arbitrary units and the horizontal scale is retention time in arbitrary units.

(Fig. 2C,D vs. 2A,B). A type 2 transferrin pattern is consistent with N-glycan remodeling defects previously described in patients with homozygous mutation in *MAN1B1* (Rymen et al. 2013).

MAN1B1 Protein Levels Were Decreased in Mutant Fibroblasts

Expression of MAN1B1 and SEC23A was examined in lysates of fibroblasts derived from skin biopsies of unaffected family members with heterozygous mutation in only *SEC23A* and heterozygous mutations in both *SEC23A* and *MAN1B1* and from affected patients (mutant fibroblasts). No significant differences were observed in the level of SEC23A in any of the samples (Fig. 3A; Supplemental Fig. S4A).

The R334C mutation in *MAN1B1* was previously demonstrated to result in a decreased level of MAN1B1 protein (Rymen et al. 2013); and we found that this was the case in fibroblasts from affected patients ($P < 0.001$, ANOVA) (Fig. 3B; Supplemental Fig. S4B). A significant decrease in MAN1B1 level was also observed in fibroblasts with heterozygous

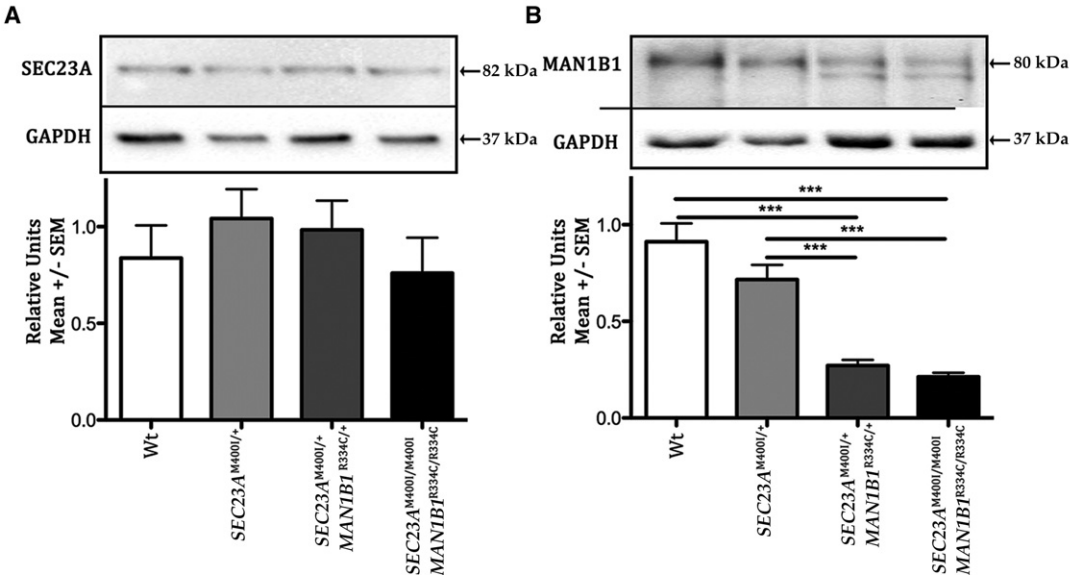

Figure 3. Representative western blot and bar graph showing expression levels of SEC23A (*A*) and MAN1B1 (*B*) proteins in wild-type (Wt); *SEC23A* $^{M400I/+}$ heterozygous; *SEC23A*$^{M400I/+}$ *MAN1B1*$^{R334C/+}$ double heterozygous; and *SEC23A*$^{M400I/M400I}$ *MAN1B1*$^{R334C/R334C}$ double homozygous mutant fibroblasts. The error bars represent standard error of the mean (SEM). Differences in protein levels were detected by one-way ANOVA (analysis of variance), followed by Tukey's multiple comparison test. GAPDH was used as an internal control. ***, $P < 0.001$.

mutations in both *SEC23A* and *MAN1B1* ($P < 0.001$, ANOVA) when compared with wild-type and *SEC23A* heterozygous fibroblasts (Fig. 3B). In addition, a smaller band of ~75 kDa was observed for MAN1B1. Thus, the 1200G>C *SEC23A* mutation does not modulate levels of SEC23A. However, the 1000C>T *MAN1B1* mutation results in decreased levels of MAN1B1 in homozygous patients as well as in unaffected carriers. In addition, this mutation generates a new or differentially modified protein product.

Dilated ER and Reduced Golgi-Associated Vesicles in Mutant Fibroblasts

Mutations in *SEC23A* are associated with abnormal dilation of the ER membranes (Boyadjiev et al. 2006, 2011), and mutations in *MAN1B1* are associated with dilation and fragmentation of the Golgi (Rymen et al. 2013); therefore, we performed transmission electron microscopy (TEM) to examine morphology of the ER and Golgi. We found that a small percentage of wild-type cells had dilated ER, whereas 100% of fibroblasts from this family were dilated (Table 4). In addition, although the ER in wild-type cells was generally contiguous, fibroblasts from the family showed fragmented and distended ER (Fig. 4, cf. B–D and A). Furthermore, Golgi in fibroblasts from all members of this family had a reduced number of associated vesicles (Fig. 4, cf. F–H and E). Thus, heterozygous mutation in *SEC23A* alone results in abnormal dilation of the ER and a reduced number of Golgi-associated vesicles.

Increased Intracellular and Secreted Pro-COL1A1 in Fibroblasts with Homozygous Mutations in Both *SEC23A* and *MAN1B1* in the Presence of L-Ascorbic Acid

SEC23A is required for normal transport of pro-COL1A1 (Boyadjiev et al. 2006, 2011), a major extracellular matrix component of bone. Therefore, we examined levels of pro-COL1A1 mRNA and protein and its secretion in cells cultured in the presence of L-ascorbic acid, a cofactor for prolyl-4-hydroxylase (P4H), which is required in fibroblast for increased production,

Table 4. Quantification of cells with dilated endoplasmic reticulum (ER) and COPII vesicles associated with Golgi by transmission electron microscopy

Genotype of cell line	Cells with dilated ER (%)	Cells with Golgi-associated vesicles (%)
Wt ($N = 414$)	2 (0.5)	309 (75)
SEC23A$^{c.1200G>C/+}$ ($N = 83$)	83 (100***)	9 (11***)
SEC23A$^{c.1200G>C/+}$ *MAN1B1*$^{c.1000C>T/+}$ ($N = 190$)	190 (100***)	3 (1.6***)
SEC23A$^{c.1200G>C/c.1200G>C}$; *MAN1B1*$^{c.1000C>T/c.1000C>T}$ ($N = 328$)	328 (100***)	2 (0.6***)

Wt, wild type; *N*, number of cells examined. ***, $P < 0.001$.

hydroxylation, and normal folding of procollagen (Berg and Prockop 1973; Jimenez et al. 1973; Blanck and Peterkofsky 1975). No significant differences were found in the mRNA levels of pro-COL1A1 in fibroblasts from this family, suggesting that these mutations do not perturb transcription of this gene (Supplemental Fig. S5).

Fibroblasts with heterozygous mutation in *SEC23A* alone had a significant increase in secreted pro-COL1A1 ($P < 0.01$, ANOVA). In addition, significantly higher levels of intracellular ($P < 0.05$, ANOVA) and secreted pro-COL1A1 ($P < 0.001$, ANOVA) were found in fibroblasts from patients with homozygous mutations in both *SEC23A* and *MAN1B1* when compared with wild type or cells with heterozygous mutations in both *SEC23A* and *MAN1B1* (Fig. 5; Supplemental Fig. S4C). A number of faster migrating bands were also observed in lysates and conditioned medium of fibroblasts with heterozygous or homozygous mutations in both genes, when compared with wild-type and *SEC23A* heterozygous fibroblasts (red asterisk), and the intensity of these bands increased when two mutant alleles of the *SEC23A* and *MAN1B1* mutations were present (Fig. 5). Our data indicate that the 1200G>C mutation in *SEC23A* results in increased pro-COL1A1 secretion and that double homozygous mutations in both *SEC23A* and *MAN1B1* result in further perturbation of pro-COL1A1 trafficking.

Localization of Pro-COL1A1 in the Early Secretory Pathway Is Disrupted in Mutant Fibroblasts

Increased intracellular level of pro-COL1A1 was found in patient fibroblasts by western blot analysis. Furthermore, as mutations in *SEC23A* are associated with abnormal accumulation of pro-COL1A1 in the ER, distribution of pro-COL1A1 in ER was investigated by double immunofluorescence confocal microscopy with antibodies against pro-COL1A1 and protein disulfide isomerase (PDI), an ER luminal protein. Colocalization of PDI and pro-COL1A1 was significantly reduced in fibroblasts with heterozygous and homozygous mutations in both *SEC23A* and *MAN1B1* ($P < 0.001$, ANOVA) when compared with colocalization in wild-type and *SEC23A* heterozygous cells (Fig. 6, cf. I,L and C,F) (Table 5; Supplemental Fig. S6). Thus, the presence of combined mutations in *SEC23A* and *MAN1B1* results in reduced pro-COL1A1 in the ER.

To determine whether increased intracellular levels of pro-COL1A1 were due to abnormal accumulation of this protein in the Golgi of mutant cells, double immunofluorescence confocal microscopy with antibodies against pro-COL1A1 and TGN38, an integral membrane protein in the *trans*-Golgi, was performed. Colocalization of pro-COL1A1 and TGN38 was significantly increased in cells with heterozygous ($P < 0.05$ ANOVA) and homozygous ($P < 0.01$, ANOVA) mutations in both genes (Fig. 7, cf. I,L and C,F) when compared with wild type and cells with heterozygous mutation in *SEC23A* (Table 5; Supplemental Fig.

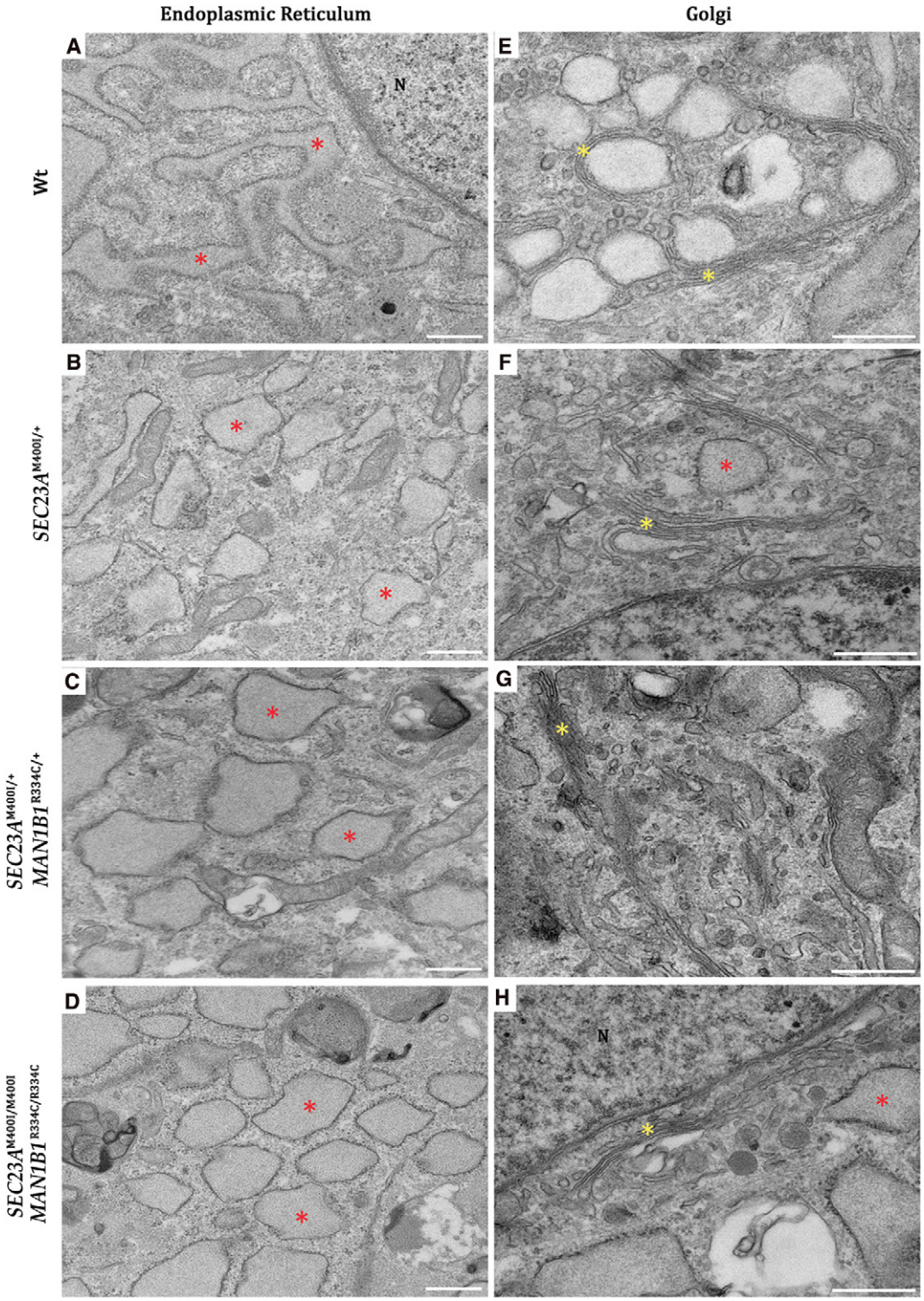

Figure 4. Dilated endoplasmic reticulum (ER) and compressed Golgi membranes with few COPII vesicles in patient fibroblasts. Representative transmission electron microscopy (TEM) images showing ER membrane (*A–D*) and Golgi (*E–H*) morphology of wild-type (Wt) (*A*,*E*); *SEC23A*$^{M400I/+}$ heterozygous (*B*,*F*); *SEC23A*$^{M400I/+}$ *MAN1B1*$^{R334C/+}$ double heterozygous (*C*,*G*); and *SEC23A*$^{M400I/M400I}$ *MAN1B1*$^{R334C/R334C}$ double homozygous mutant (*D*,*H*) fibroblasts. Magnification panels and scale bar are shown at (*A–D*) 9300× and 0.5 µm, respectively; (*E–H*) 13000× and 0.5 µm, respectively. A red asterisk represents dilated ER membrane and a yellow asterisk represents Golgi.

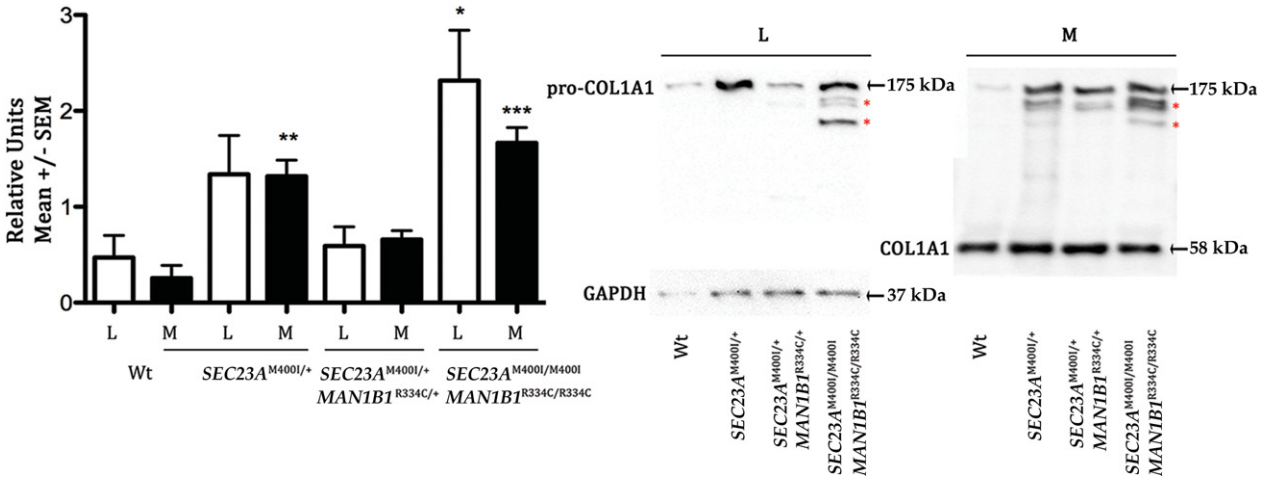

Figure 5. Pro-COL1A1 production and secretion in fibroblasts with mutations in *SEC23A* and *MAN1B1*. Bar graph and representative western blots showing expression of pro-COL1A1 protein in cell lysate (L) versus conditioned media (M) in wild-type (Wt); *SEC23A*$^{M400I/+}$ heterozygous; *SEC23A*$^{M400I/+}$ *MAN1B1*$^{R334C/+}$ double heterozygous; and *SEC23A*$^{M400I/M400I}$ *MAN1B1*$^{R334C/R334C}$ double homozygous fibroblasts. A red asterisk represents additional smaller bands observed for pro-COL1A1 in double homozygous samples. Error bars represent standard error of the mean (SEM). Differences in protein levels were detected by one-way ANOVA analysis, followed by Tukey's multiple comparison test. *, $P < 0.05$; **, $P < 0.01$; and ***, $P < 0.001$.

S6). Thus, combined mutations in *SEC23A* and *MAN1B1* result in retention of pro-COL1A1 in the Golgi.

Mutations in *SEC23A* and *MAN1B1* Result in Increased Secretion of Pro-COL1A1 in the Absence of L-Ascorbic Acid

Iannotti et al. (2014) recently reported a nonenzymatic requirement for MAN1B1 in quality control to prevent secretion of abnormally folded proteins. Fibroblasts with heterozygous and homozygous mutations in both *SEC23A* and *MAN1B1* have decreased levels of MAN1B1 protein, but only homozygous patients have glycosylation defects (consistent with reduced MAN1B1 enzymatic activity). We examined intracellular and secreted levels of pro-COL1A1 in the absence of L-ascorbic acid, which is required for folding of the collagen triple helix (Walmsley et al. 1999), to determine whether quality control of this protein is disrupted in fibroblasts with mutations in *MAN1B1*. In the absence of L-ascorbic acid, pro-COL1A1 is not secreted but retained in the ER and/or degraded in wild-type fibroblasts. Fibroblasts heterozygous for the *SEC23A* mutation had nonsignificant increases of intracellular and secreted pro-COL1A1. However, significantly more pro-COL1A1 was secreted in fibroblasts with heterozygous mutations in both *SEC23A* and *MAN1B1* ($P < 0.05$, ANOVA), when compared with wild type (Supplemental Fig. S7). Surprisingly, mutant fibroblasts showed levels of intracellular and secreted pro-COL1A1 comparable with those of wild-type cells. Our data indicate that a normal level of MAN1B1 is required to prevent secretion of abnormally folded pro-COL1A1. These data also indicate that an alternate pathway is used for quality control of pro-COL1A1 when MAN1B1 α-mannosidase activity is reduced.

DISCUSSION

In this study, we describe identification and characterization of abnormalities in patients with homozygous mutations in two genes, a novel mutation in *SEC23A*, 1200G>C and a

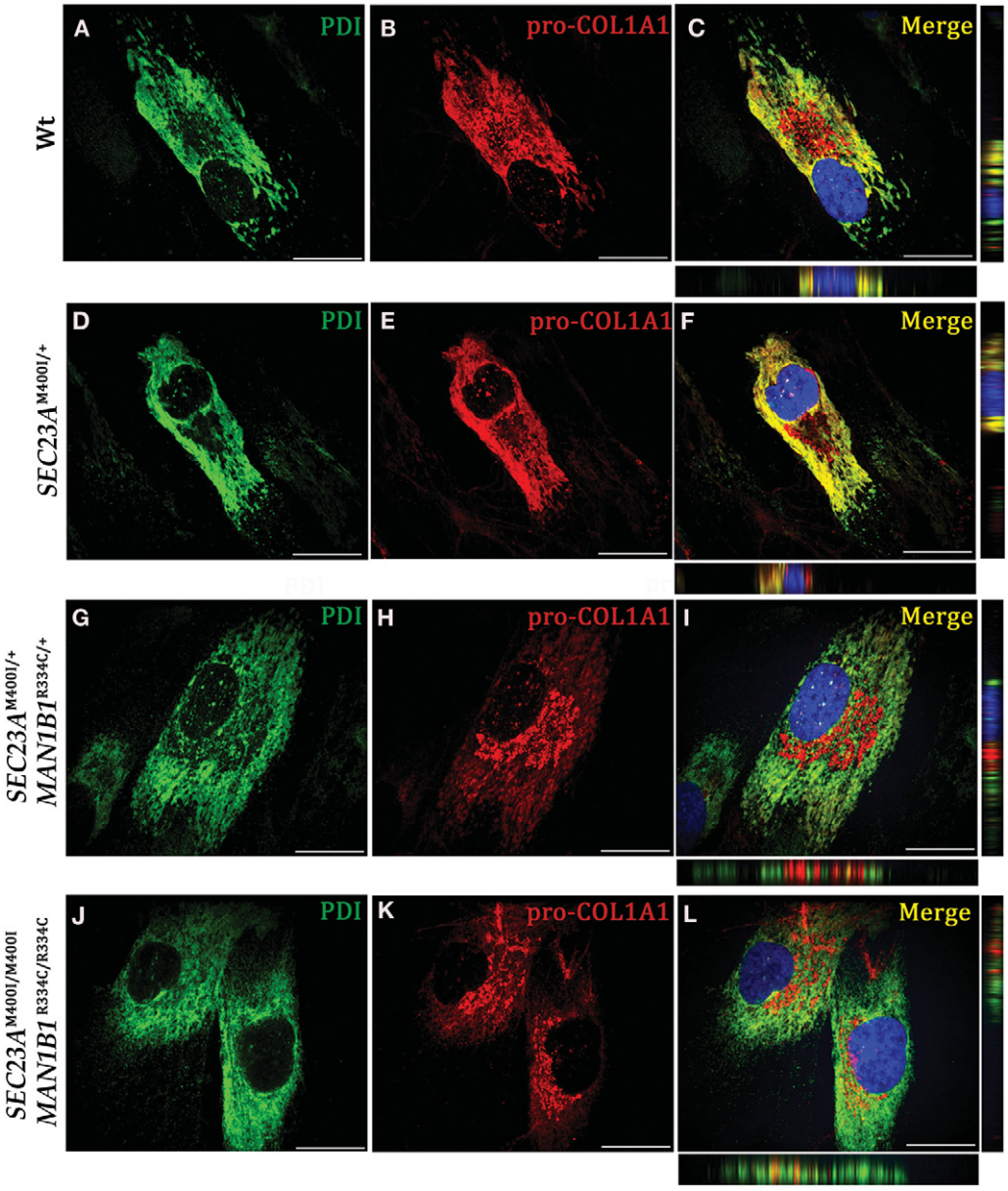

Figure 6. Colocalization of pro-COL1A1 with endoplasmic reticulum (ER) was reduced in patient fibroblasts. Protein disulfide isomerase (PDI) (green; *A*,*D*,*G*,*J*), a marker of ER lumen, and intracellular pro-COL1A1 (red; *B*, *E*,*H*,*K*) were visualized using immunofluorescence microscopy. Merged images showing pro-COL1A1 colocalization with PDI in wild-type (Wt) (*C*); *SEC23A*$^{M400I/+}$ heterozygous (*F*); *SEC23A*$^{M400I/+}$ *MAN1B1*$^{R334C/+}$ double heterozygous (*I*); and *SEC23A*$^{M400I/M400I}$ *MAN1B1*$^{R334C/R334C}$ double homozygous (*L*) fibroblasts. Each representative image is a *z*-stack projection of three optical sections. *x*–*z* and *y*–*z* projection of merged images are also shown. Scale bar, 20 µm.

previously identified mutation in *MAN1B1*, 1000C>T. The affected patients presented with moderate global developmental delay, tall stature, obesity, macrocephaly, mild dysmorphic features, hypertelorism, malocclusion teeth, intellectual disability, and flat feet. We found that mutations in the two genes segregated in the family and that the unaffected parents were healthy and carried heterozygous mutations in both *SEC23A* and *MAN1B1*, consistent

Table 5. Statistical analysis of pro-COL1A1 colocalization with endoplasmic reticulum (ER) or *trans*-Golgi by confocal microscopy

Genotype of cell line	Manders coefficient (M2)	
	ER (PDI) overlapping pro-COL1A1	*trans*-Golgi (TGN38) overlapping pro-COL1A1
Wt	0.86 ($N = 19$)	0.11 ($N = 27$)
SEC23A$^{c.1200G>C/+}$	0.79 ($N = 16$)	0.13 ($N = 28$)
SEC23A$^{c.1200G>C/+}$ *MAN1B1*$^{c.1000C>T/+}$	0.69*** ($N = 59$)	0.17* ($N = 150$)
SEC23A$^{c.1200G>C/c.1200G>C}$, *MAN1B1*$^{c.1000C>T/c.1000C>T}$	0.73*** ($N = 41$)	0.18** ($N = 138$)

PDI, protein disulfide isomerase; TGN38, trans-Golgi integral membrane protein 38; Wt, wild type; *N*, the number of cells examined. *, $P < 0.05$; **, $P < 0.01$; ***, $P < 0.001$.

with an autosomal-recessive mode of inheritance. We also identified heterozygous mutation in *SEC23A* in an unaffected sibling of tall stature and normal intelligence. Fibroblasts were isolated and used to characterize cellular abnormalities associated with these mutations and to confirm contribution of both mutations to abnormal protein transport. We propose that homozygosity for both of these mutations in *SEC23A* and *MAN1B1* explains a subset of phenotypic abnormalities found in the affected boys. These findings are consistent with a previously undescribed digenic phenotype in the two affected patients.

Mutations in either *SEC23A* (seven cases reported from two families) or *MAN1B1* (19 cases reported from 11 families) in humans are rare; thus, it is surprising to find mutations in both *SEC23A* and *MAN1B1* as we are reporting here (two cases from one family). Patients with mutations in either *SEC23A* or *MAN1B1* share some phenotypic similarities—for example, both are described as short, they present with developmental delay, hypertelorism, thin upper lip, joint hypermobility, intellectual disability, and obesity (Table 3). However, although the patients we describe with homozygous mutation in both *SEC23A* and *MAN1B1* share many features with *SEC23A* or *MAN1B1* homozygous patients, a few phenotypes were novel. For example, *SEC23A* and *MAN1B1* homozygous patients are tall; in contrast *SEC23A* or *MAN1B1* homozygous patients are short (Table 3). In addition, although Patients 1 and 2 as well as patients with mutations in *SEC23A* have dental abnormalities, our affected patients have large and malocclusion teeth, whereas patients with *SEC23A* homozygous mutation had delayed tooth eruption and dental caries. These novel phenotypes are most likely due to the combined abnormalities in protein transport and glycosylation.

SEC23A functions as a GAP for SAR1 to regulate coat protein assembly and disassembly (Yoshihisa et al. 1993). The F382L SEC23A mutation, which disrupts SEC23A interaction with SEC31, provided the first evidence that SEC23A was important for pro-COL1A1 transport (Boyadjiev et al. 2006). Further evidence for this was provided by knockdown of SEC13, another interacting partner of SEC31 (Townley et al. 2008), and by the finding of abnormal pro-COL1A1 retention in the ER as a consequence of the M702V SEC23A mutation (Boyadjiev et al. 2011; Kim et al. 2012). The previously identified mutations in *SEC23A* are predicted to reduce availability of COPII proteins on ER membranes and consequently prevent or delay transport of pro-COL1A1 (Kim et al. 2012).

Our data indicate that the novel M400I SEC23A mutation also perturbs pro-COL1A1 transport but via a novel mechanism. This mutation, for example, results in increased secretion of pro-COL1A1, and although ER membranes are dilated, the numbers of Golgi-associated vesicles are decreased, and pro-COL1A1 is not abnormally retained in the ER. Thus, the mechanism via which SEC23A results in increased pro-COL1A1 secretion is not clear. Nonetheless, a genetic interaction between *MAN1B1* and *SEC23A* is indicated, and cells

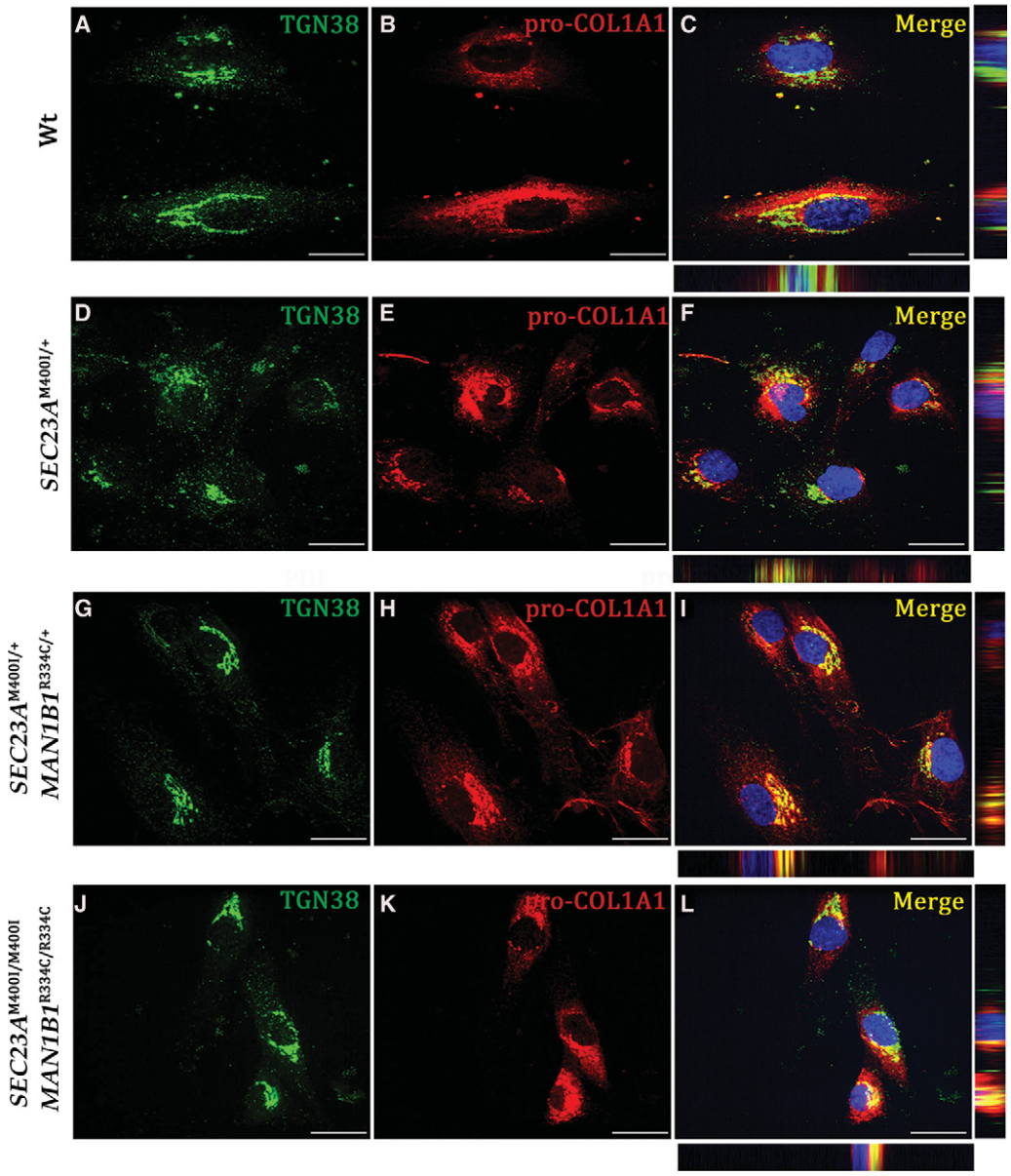

Figure 7. Colocalization of pro-COL1A1 with *trans*-Golgi was increased in patient fibroblasts. TGN38 (green; *A*,*D*,*G*,*J*), a marker of *trans*-Golgi, and intracellular pro-COL1A1 (red; *B*,*E*,*H*, *K*) were visualized using immunofluorescence microscopy. Merged images showing pro-COL1A1 colocalization with TGN38 in wild-type (*C*); *SEC23A*$^{M400I/+}$ heterozygous (*F*); *SEC23A*$^{M400I/+}$ *MAN1B1*$^{R334C/+}$ double heterozygous (*I*); and *SEC23A*$^{M400I/M400I}$ *MAN1B1*$^{R334C/R334C}$ double-homozygous (*L*) fibroblasts. Each representative image is a *z*-stack projection of three optical sections. *x*–*z* and *y*–*z* projections of merged images are also shown. Scale bar, 20 µm.

with mutations in both *SEC23A* and *MAN1B1* showed decreased levels of pro-COL1A1 in the ER and its retention in the Golgi. Decreased levels of pro-COL1A1 in the ER may be due to perturbed interactions between SEC23A and accessory proteins required for efficient COPII vesicle formation and/or collagen secretion (Wilson et al. 2011; Lord et al. 2013). We postulate that pro-COL1A1 is more efficiently packaged into COPII vesicles because of the

SEC23A mutation, but that retrograde transport from the Golgi is perturbed when *MAN1B1* is mutated, as previously suggested by Iannotti et al. (2014).

The 1000C>T mutation in *MAN1B1* was previously shown to result in decreased MAN1B1 protein levels and to encode for an enzyme with reduced catalytic function (Rafiq et al. 2011; Rymen et al. 2013). Rymen et al. (2013) also showed that patients with this mutation had abnormal N-glycan remodeling. Our data are consistent with those of Rafiq et al. and Rymen et al., as we found reduced MAN1B1 protein levels and glycosylation defects in patients double homozygous for the 1000C>T *MAN1B1* and the 12000 G>C *SEC23A* mutations. However, although we also found reduced levels of MAN1B1 protein in fibroblasts of unaffected carriers, MAN1B1 α-mannosidase activity in these patients must be sufficient, because they did not have glycosylation defects. Also, we postulate that additional bands (below the expected band) of MAN1B1, found in double heterozygous and double homozygous mutant fibroblasts, may represent a novel protein product generated as a consequence of the 1000C>T *MAN1B1* mutation, although we cannot rule out that this band represents a deglycosylated isoform of MAN1B1.

In a recent report, Iannotti et al. showed a role for MAN1B1 in retention and ERAD of abnormally folded proteins from the Golgi to the ER, independent of its mannosidase activity. The authors suggest that abnormalities in patients with *MAN1B1* mutations could be due to a combination of reduced enzymatic activity and quality control (Iannotti et al. 2014). Our study confirms a requirement for wild-type levels of MAN1B1 protein for quality control. Secretion of pro-COL1A1 was increased in cells with heterozygous mutations in both *SEC23A* and *MAN1B1* in the absence of ascorbic acid, suggesting that abnormally folded protein is secreted from these cells. However, decreased quality control alone is not sufficient to cause disease in unaffected carriers; thus, we propose that it is reduced α-mannosidase activity and the ensuing glycosylation defects that result in morphological abnormalities in patients with homozygous mutations in *MAN1B1*. Furthermore, because secretion of abnormally folded pro-COL1A1 is reduced in cells with homozygous mutations in both genes, in the absence of ascorbic acid, an unknown pathway is utilized for quality control when α-mannosidase activity is decreased, implying a role for the enzymatic activity of MAN1B1 in quality control.

Nonetheless, we cannot rule out the possibility that *MAN1B1* homozygous fibroblasts generate a procollagen1 protein with altered stability and modified interactions with procollagen, COL2A1 (OMIM #120140), a different procollagen associated with skeletal abnormalities including tall stature (Bleasel et al. 1995). Furthermore, although mutation in another α-mannosidase, *MAN2B1*, is associated with tall stature (OMIM #248500), we found that increased pro-COL1A1 secretion segregated with tall stature in the heterozygous sister suggests that it is *SEC23A* mutation that is responsible for this aspect of the phenotype. Future studies will focus on determining how double homozygous mutations in *SEC23A* (1200G>C) and *MAN1B1* (1000C>T) result in increased intracellular pro-COL1A1 levels and increased pro-COLA1 secretion.

The disease described in the two affected patients is a clear example of digenic inheritance (DI) disease, as described by Schaffer. DI in human is a case where "the variant genotypes at two loci explain the phenotypes of some patients and their unaffected (or more mildly affected) relatives more clearly than the genotypes at one locus alone" (Schaffer 2013). In this article, we describe two patients with homozygous mutations in both *MAN1B1* and *SEC23A*. Although only the *MAN1B1* mutation was previously shown to be disease-causing, we show that mutation in *SEC23A* alone segregates in the family with tall stature and perturbs pro-COL1A1 transport. We do not think that reduced penetrance or variable expressivity of the *MAN1B1* mutation can account for differences in phenotype of patients in this study compared with previously described patients with mutation in *MAN1B1*—for example, all patients with *MAN1B1* mutations to date are significantly short (Rafiq et al. 2011; Rymen et al. 2013; Van Scherpenzeel et al. 2014), unlike these two patients. Our

findings are most consistent with contribution of the novel mutation in *SEC23A* to the phenotype of these two patients. However, because patients with this *SEC23A* (1200G>C) alone have not been reported, we cannot rule out that this is a case of two Mendelian diseases. Our work suggests that WES of patients with common (i.e., less rare) autosomal diseases, like thalassemia or cystic fibrosis, may help to uncover the genetic basis of atypical phenotypes, as we have previously done for 22q11.2DS (McDonald-McGinn et al. 2013).

METHODS

Subjects and Sample Preparation

Skin biopsies of affected patients and unaffected family members were used to generate fibroblast cells using standard conditions (Shih et al. 1989). Ethnically matched wild-type fibroblasts were provided as a gift from Dr. Nancy Braverman and Dr. Indra Gupta. Fibroblasts were cultured in Dulbecco's modified Eagle's medium (DMEM) with 10% fetal bovine serum. For procollagen1 experiments, fibroblasts were cultured in DMEM media supplemented with or without L-ascorbic acid (50 µg/mL).

Exome Capture and Sequencing

WES analysis was performed as previously described (McDonald-McGinn et al. 2013; Fahiminiya et al. 2014) at the Genome Quebec Innovation Center, Montreal, Canada. In brief, 3 µg of genomic DNA was used for library preparation and exome capturing of Patients 1 and 2 using the Illumina TruSeq Exome Enrichment Kit and the Agilent SureSelect Human All Exon kit version 4, respectively. Subsequently, the captured exons were sequenced on an Illumina HiSeq2000 sequencer with read lengths of 100 bp. BWA (Burrows–Wheeler Aligner) (v. 0.5.9) (Li and Durbin 2009), GATK (Genome Analysis Toolkit) (version 1.0.5083) (McKenna et al. 2010), SAMtools mpileup (v. 0.1.17) (Li et al. 2009), and ANNOVAR (Wang et al. 2010) were used for alignment, indel realignment, variant calling, and annotation, respectively. The human reference genome (GRCh37/hg19) was considered for all analyses. A mean coverage of 80× (Patient 1) and 142× (Patient 2) was obtained for all consensus coding sequence (CCDS) exons and >85% of CCDS bases were covered by at least 10 reads. To focus on the most likely disease-causing variants, those that had an allele frequency >5% in the 1000 Genomes Project (http://www.1000genomes.org) and the NHLBI GO Exome Sequencing (ESP) databases and observed in more than seven individuals in our in-house exome database (more than 1400 exomes) were filtered out. Mutations were identified in five genes *MUM1L1* (GenBank accession # NM_152423.4), *NUP214* (GenBank accession # NM_005085.3), *SASH3* (GenBank accession # NM_018990.3), *SEC23A* (GenBank accession # NM_006364.2), and *MAN1B1* (GenBank accession # NM_016219.4) (Supplemental Table 1). Finally, the variants that were predicted to be the most likely protein-damaging by three different bioinformatics algorithms—SIFT (http://sift.jcvi.org/) (Kumar et al. 2009), PolyPhen-2 (http://genetics.bwh.harvard.edu/pph2/) (Adzhubei et al. 2010), and MutationTaster (http:// www.mutationtaster.org/) (Schwarz et al. 2014)—were validated using Sanger sequencing and considered for further analysis. cDNA numbering of mutations was used: +1 represents the A of the ATG translation codon in the reference sequence, with the initiation codon as codon 1.

Capillary Zone Electrophoresis

The serum samples were run as described previously (Parente et al. 2010).

Western Blot Analysis

Western blot analysis was performed according to standard protocols and as previously described (Jerome-Majewska et al. 2010). Briefly, lysates were collected from fibroblasts in 1× RIPA lysis buffer. Equivalent amounts of protein were resolved on sodium dodecyl sulfate polyacrylamide gel electrophoresis (SDS-PAGE) and transferred to polyvinylidene fluoride (PVDF membrane, Bio-Rad). Membranes were blocked with 5% nonfat dry milk in TBST (Tris-buffered saline with Tween 20) and incubated with first primary and then secondary antibodies. The immunoreactive bands were detected by the ECL plus Western Blotting Detection System (GE Healthcare). All western blots were repeated at least three times on lysates collected from three different cellular passes. The western blots images were taken with Bio-Rad's ChemiDoc MP System (catalog # 1708280), and bands were digitally analyzed using ImageJ software. The following primary antibodies were used: SEC23A rabbit monoclonal antibody (1:5000, a gift from Dr. Randy Schekman), MAN1B1 mouse monoclonal antibody (1:5000, a gift from Dr. Richard N. Sifers), LF-68 (human αI(1) carboxy-telopeptide) anti-Pro-COL1A1 rabbit serum (a gift from L.W. Fisher, National Institutes of Health [NIH]) (Fisher et al. 1995), and GAPDH rabbit monoclonal antibody (1:10,000, Cell Signaling, catalog # 2118), as a loading control. All bands detected with the Pro-COL1A1 antibody were quantified as pro-COL1A1 for western blots shown in Figure 5 and Supplemental Fig. S5. The secondary antibodies goat anti-rabbit secondary antibody (Cell Signaling; catalog # 7074) and goat anti-mouse secondary antibody (Cell Signaling; catalog # 7076) were used.

Transmission Electron Microscopy (TEM)

Fibroblasts were cultured to 70% confluence, washed with phosphate buffered saline (PBS), fixed with 25% glutaraldehyde in 0.1 M cacodylate buffer (pH = 7.5), stained in 2% reduced osmium tetraoxide, and embedded in Epone. The samples were sectioned at the McGill FEMR facility. Imaging of sections was completed on the Tecnai T12 120 kV TEM microscope. For quantification, four grids per patient line and six grids per control line were examined in their entirety to obtain a representation of the cellular morphology. The cells used for quantification had at least 75% of their cellular volume clearly visible. Dilation of the ER was recorded when >75% of the ER membranes in the cell were dilated.

RNA Isolation and Quantitative RT-PCR

RNA was isolated from fibroblasts in TRIzol reagent according to the manufacturer's instruction, as previously described (Jerome-Majewska et al. 2010). Reverse transcription was performed with iScript cDNA synthesis kit according to the manufacturer's instruction (Bio-Rad, Cat. #170-8890). The QuantiFast SYBR Green PCR kit (QIAGEN, Cat. #204054) was used for quantitative reverse transcription–polymerase chain reaction (qRT-PCR) in a LightCycler 480 II (Roche). The cycling conditions included a hot start at 95°C for 5 min, followed by 40 cycles at 95°C for 10 sec and 60°C for 30 sec. *GAPDH* was used as a reference gene for qRT-PCR. Relative gene expression was determined by using $2^{-\Delta\Delta CT}$ according to standard methods (Bio-Rad). These experiments were repeated at least two times on lysates collected from two different cellular passes. The following primers were used: GAPDH (5′-GCA GGG GGG AGC CAA AAG GGT-3′, 5′-TGG GT GCA GTG ATG GCA TGG-3′) and pro-COL1A1 (5′-CCT ACA TGG ACC AGC AGA CT-3′, 5′-GGA GGT CTT GGT GGT TTT G-3′).

Immunofluorescence Microscopy

Immunofluorescence was performed according to standard protocols and as previously described (Zakariyah et al. 2012). Briefly, fibroblasts were seeded in eight-well chamber slides (Thermo Fisher Scientific; catalog # 154534) for 48 h in DMEM media, rinsed with PBS, fixed with 3% paraformaldehyde (PFA) for 10 min, and permeabilized in 0.5% Triton X-100 for

3 min. Cells were blocked with 5% goat serum and incubated with first primary and then secondary antibodies (diluted in PBS). VECTASHIELD Hard Set Mounting Medium containing DAPI (4′,6-diamidino-2-phenylindole) (Vector; catalog # H-1500) was used to counterstain nuclei. The following primary antibodies were used for immunofluorescence: Anti-PDI [RL90] (1:100; Abcam; catalog # ab2792-100), Anti-TGN38 [21-G (1:250; Santa Cruz Biotechnology; catalog # sc-101273), and LF-68 anti-Pro-COL1A1 rabbit serum (1:200, a gift from L.W. Fisher, National Institutes of Health [NIH]) (Fisher et al. 1995). Goat anti-mouse IgG 488 (Alexa-Fluor, Invitrogen) and goat anti-rabbit IgG 568 (Alexa-Fluor, Invitrogen) were used as secondary antibodies. Images were recorded with an Olympus 1X81 confocal microscope. The overlap of two proteins on each section was analyzed by Mander's coefficient for green (M1) and red (M2) separately. Colocalization of pro-COL1A1 and PDI or pro-COL1A1 and TGN38 was analyzed from two independent experiments.

Statistical Analysis

Group data were expressed as mean ± standard error of the mean (SEM) from at least three independent experiments. Statistical analysis was performed using one-way ANOVA followed by the Tukey–Kramer multiple comparison test at a level of significance of $P < 0.05$ using Prism software. The *P*-values are represented as * for <0.05, and ** for <0.01, and *** for <0.001. Graphs were plotted with Prism software.

ADDITIONAL INFORMATION

Ethics Statement

Patients and unaffected family members gave written informed consent for the use of their tissues in this study and for publication of de-identified data and photos. The institutional review board of UBC approved this study under study number H10-03215.

Data Deposition and Access

Variants reported in this manuscript have been submitted to the LOVD (Leiden Open Variation Database) database (http://www.lovd.nl/3.0/home) and can be accessed at http://databases.lovd.nl/shared/variants/SEC23A (*SEC23A*), http://databases.lovd.nl/shared/variants/MAN1B1 (*MAN1B1*), http://databases.lovd.nl/shared/variants/MUM1L1 (*MUM1L1*), http://databases.lovd.nl/shared/variants/nup214 (*NUP214*), and http://databases.lovd.nl/shared/variants/sash3 (*SASH3*). Sequencing data are not available because patient consent could not be obtained.

Acknowledgments

We would like to acknowledge Ali Fazel in the laboratory of Dr. John Bergeron, Mihaela Pupavac in the laboratory of Dr. David Rosenblatt, and Ayumu Sugiura in the laboratory of Dr. Heidi McBride for technical assistance. We also wish to acknowledge the contribution of the high-throughput sequencing platform of the McGill University and Genome Québec Innovation Centre (Montréal, Canada) and Dr. Jacek Majewski for his help in analyzing the exome data. We would also like to thank Dr. Randy Schekman, Dr. Richard N. Sifers, L.W. Fisher, and Dr. Heidi McBride for sharing their antibodies.

Author Contributions

S.G. and L.A.J-M. designed the study and wrote the paper. W.T.G. analyzed the clinical features of patients. S.F. and L.D.N. performed and analyzed the whole-exome sequencing results. B.G. conceived and analyzed the capillary zone electrophoresis experiments. T.W.

performed and analyzed the transmission electron microscopy data. J.J.M.B. analyzed the transmission electron microscopy. S.G. performed and analyzed the western blot, qRT-PCR, and immunofluorescence microscopy experiments. D.S.R. and J.J.M.B critically reviewed the manuscript. S.G. and L.A.J-M. approved the final version of the manuscript.

Competing Interest Statement

The authors have declared no competing interest.

Received October 22, 2015; accepted in revised form December 31, 2015.

Funding

This work was supported by a grant from the Canadian Institutes of Health Research (MOP-102666 to L.A.J-M.). L.A.J-M., D.S.R., B.M.G., and J.J.M.B. are members of the Research Institute of the McGill University Health Centre, which is supported in part by the Fonds de Recherché Santé.

REFERENCES

Adzhubei IA, Schmidt S, Peshkin L, Ramensky VE, Gerasimova A, Bork P, Kondrashov AS, Sunyaev SR. 2010. A method and server for predicting damaging missense mutations. *Nat Methods* **7:** 248–249.

Beer S, Scheikl T, Reis B, Huser N, Pfeffer K, Holzmann B. 2005. Impaired immune responses and prolonged allograft survival in *Sly1* mutant mice. *Mol Cell Biol* **25:** 9646–9660.

Berg RA, Prockop DJ. 1973. The thermal transition of a non-hydroxylated form of collagen. Evidence for a role for hydroxyproline in stabilizing the triple-helix of collagen. *Biochem Biophys Res Commun* **52:** 115–120.

Blanck TJ, Peterkofsky B. 1975. The stimulation of collagen secretion by ascorbate as a result of increased proline hydroxylation in chick embryo fibroblasts. *Arch Biochem Biophys* **171:** 259–267.

Bleasel JF, Bisagni-Faure A, Holderbaum D, Vacher-Lavenu MC, Haqqi TM, Moskowitz RW, Menkes CJ. 1995. Type II procollagen gene (COL2A1) mutation in exon 11 associated with spondyloepiphyseal dysplasia, tall stature and precocious osteoarthritis. *J Rheumatol* **22:** 255–261.

Boyadjiev SA, Fromme JC, Ben J, Chong SS, Nauta C, Hur DJ, Zhang G, Hamamoto S, Schekman R, Ravazzola M, et al. 2006. Cranio-lenticulo-sutural dysplasia is caused by a *SEC23A* mutation leading to abnormal endoplasmic-reticulum-to-Golgi trafficking. *Nat Genet* **38:** 1192–1197.

Boyadjiev SA, Kim SD, Hata A, Haldeman-Englert C, Zackai EH, Naydenov C, Hamamoto S, Schekman RW, Kim J. 2011. Cranio-lenticulo-sutural dysplasia associated with defects in collagen secretion. *Clin Genet* **80:** 169–176.

Fahiminiya S, Almuriekhi M, Nawaz Z, Staffa A, Lepage P, Ali R, Hashim L, Schwartzentruber J, Abu Khadija K, Zaineddin S, et al. 2014. Whole exome sequencing unravels disease-causing genes in consanguineous families in Qatar. *Clin Genet* **86:** 134–141.

Fisher LW, Stubbs JT III, Young MF. 1995. Antisera and cDNA probes to human and certain animal model bone matrix noncollagenous proteins. *Acta Orthop Scand Suppl* **266:** 61–65.

Iannotti MJ, Figard L, Sokac AM, Sifers RN. 2014. A Golgi-localized mannosidase (MAN1B1) plays a non-enzymatic gatekeeper role in protein biosynthetic quality control. *J Biol Chem* **289:** 11844–11858.

Jerome-Majewska LA, Achkar T, Luo L, Lupu F, Lacy E. 2010. The trafficking protein Tmed2/p24β_1 is required for morphogenesis of the mouse embryo and placenta. *Dev Biol* **341:** 154–166.

Jimenez S, Harsch M, Rosenbloom J. 1973. Hydroxyproline stabilizes the triple helix of chick tendon collagen. *Biochem Biophys Res Commun* **52:** 106–114.

Kim SD, Pahuja KB, Ravazzola M, Yoon J, Boyadjiev SA, Hammamoto S, Schekman R, Orci L, Kim J. 2012. The [corrected] SEC23-SEC31 [corrected] interface plays critical role for export of procollagen from the endoplasmic reticulum. *J Biol Chem* **287:** 10134–10144.

Kumar P, Henikoff S, Ng PC. 2009. Predicting the effects of coding non-synonymous variants on protein function using the SIFT algorithm. *Nat Protoc* **4:** 1073–1081.

Li H, Durbin R. 2009. Fast and accurate short read alignment with Burrows–Wheeler transform. *Bioinformatics* **25:** 1754–1760.

Li H, Handsaker B, Wysoker A, Fennell T, Ruan J, Homer N, Marth G, Abecasis G, Durbin R. 2009. The sequence alignment/map format and SAMtools. *Bioinformatics* **25:** 2078–2079.

Lord C, Bhandari D, Menon S, Ghassemian M, Nycz D, Hay J, Ghosh P, Ferro-Novick S. 2011. Sequential interactions with Sec23 control the direction of vesicle traffic. *Nature* **473:** 181–186.

Lord C, Ferro-Novick S, Miller EA. 2013. The highly conserved COPII coat complex sorts cargo from the endoplasmic reticulum and targets it to the Golgi. *Cold Spring Harb Perspect Biol* **5:** a013367.

McDonald-McGinn DM, Fahiminiya S, Revil T, Nowakowska BA, Suhl J, Bailey A, Mlynarski E, Lynch DR, Yan AC, Bilaniuk LT, et al. 2013. Hemizygous mutations in SNAP29 unmask autosomal recessive conditions and contribute to atypical findings in patients with 22q11.2DS. *J Med Genet* **50:** 80–90.

McKenna A, Hanna M, Banks E, Sivachenko A, Cibulskis K, Kernytsky A, Garimella K, Altshuler D, Gabriel S, Daly M, et al. 2010. The Genome Analysis Toolkit: a MapReduce framework for analyzing next-generation DNA sequencing data. *Genome Res* **20:** 1297–1303.

Pan S, Wang S, Utama B, Huang L, Blok N, Estes MK, Moremen KW, Sifers RN. 2011. Golgi localization of ERManI defines spatial separation of the mammalian glycoprotein quality control system. *Mol Biol Cell* **22:** 2810–2822.

Pan S, Cheng X, Sifers RN. 2013. Golgi-situated endoplasmic reticulum α-1, 2-mannosidase contributes to the retrieval of ERAD substrates through a direct interaction with γ-COP. *Mol Biol Cell* **24:** 1111–1121.

Parente F, Ah Mew N, Jaeken J, Gilfix BM. 2010. A new capillary zone electrophoresis method for the screening of congenital disorders of glycosylation (CDG). *Clin Chim Acta* **411:** 64–66.

Rafiq MA, Kuss AW, Puettmann L, Noor A, Ramiah A, Ali G, Hu H, Kerio NA, Xiang Y, Garshasbi M, et al. 2011. Mutations in the α1,2-mannosidase gene, *MAN1B1*, cause autosomal-recessive intellectual disability. *Am J Hum Genet* **89:** 176–182.

Rymen D, Peanne R, Millon MB, Race V, Sturiale L, Garozzo D, Mills P, Clayton P, Asteggiano CG, Quelhas D, et al. 2013. MAN1B1 deficiency: an unexpected CDG-II. *PLoS Genet* **9:** e1003989.

Schaffer AA. 2013. Digenic inheritance in medical genetics. *J Med Genet* **50:** 641–652.

Schwarz JM, Cooper DN, Schuelke M, Seelow D. 2014. MutationTaster2: mutation prediction for the deep-sequencing age. *Nat Methods* **11:** 361–362.

Shih VE, Axel SM, Tewksbury JC, Watkins D, Cooper BA, Rosenblatt DS. 1989. Defective lysosomal release of vitamin B12 (cb1F): a hereditary cobalamin metabolic disorder associated with sudden death. *Am J Med Genet* **33:** 555–563.

Smirle J, Au CE, Jain M, Dejgaard K, Nilsson T, Bergeron J. 2013. Cell biology of the endoplasmic reticulum and the Golgi apparatus through proteomics. *Cold Spring Harb Perspect Biol* **5:** a015073.

Townley AK, Feng Y, Schmidt K, Carter DA, Porter R, Verkade P, Stephens DJ. 2008. Efficient coupling of Sec23-Sec24 to Sec13-Sec31 drives COPII-dependent collagen secretion and is essential for normal craniofacial development. *J Cell Sci* **121:** 3025–3034.

Van Scherpenzeel M, Timal S, Rymen D, Hoischen A, Wuhrer M, Hipgrave-Ederveen A, Grunewald S, Peanne R, Saada A, Edvardson S, et al. 2014. Diagnostic serum glycosylation profile in patients with intellectual disability as a result of MAN1B1 deficiency. *Brain* **137:** 1030–1038.

Walmsley AR, Batten MR, Lad U, Bulleid NJ. 1999. Intracellular retention of procollagen within the endoplasmic reticulum is mediated by prolyl 4-hydroxylase. *J Biol Chem* **274:** 14884–14892.

Wang K, Li M, Hakonarson H. 2010. ANNOVAR: functional annotation of genetic variants from high-throughput sequencing data. *Nucleic Acids Res* **38:** e164.

Wilson DG, Phamluong K, Li L, Sun M, Cao TC, Liu PS, Modrusan Z, Sandoval WN, Rangell L, Carano RA, et al. 2011. Global defects in collagen secretion in a *Mia3/TANGO1* knockout mouse. *J Cell Biol* **193:** 935–951.

Yoshihisa T, Barlowe C, Schekman R. 1993. Requirement for a GTPase-activating protein in vesicle budding from the endoplasmic reticulum. *Science* **259:** 1466–1468.

Zakariyah A, Hou W, Slim R, Jerome-Majewska L. 2012. TMED2/p24β1 is expressed in all gestational stages of human placentas and in choriocarcinoma cell lines. *Placenta* **33:** 214–219.